RESEARCH REPORT VTT-R-00113-25

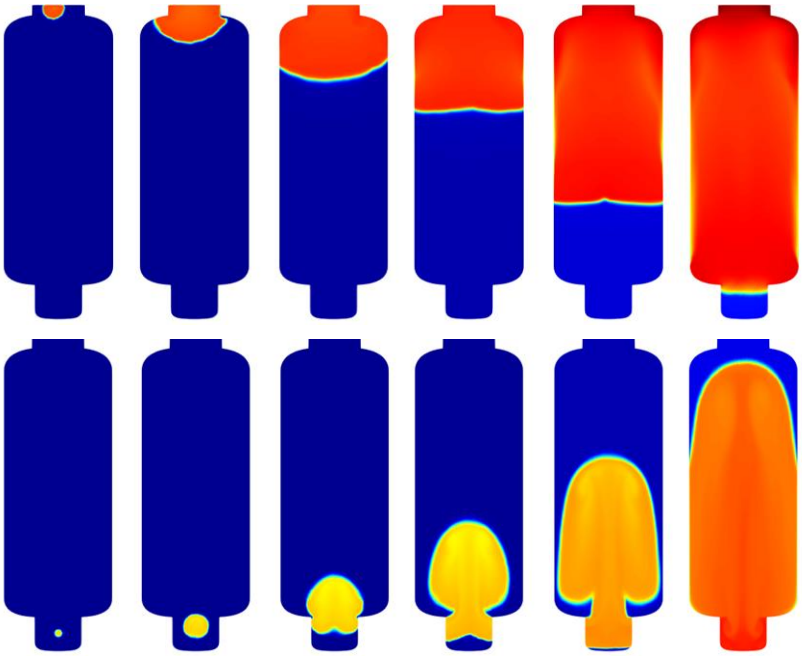

Modelling of hydrogen deflagration with OpenFOAM *XiFluid* solver

Authors: Johanna Kapanen

Confidentiality: VTT Public

Version: 26.3.2025

VTT

beyond the obvious

Report's title	
Modelling of hydrogen deflagration with OpenFOAM *XiFluid* solver	
Customer, contact person, address Valtion Ydinjätehuoltorahasto Linda Kumpula (Työ- ja elinkeinoministeriö) PL 32, 00023 Valtioneuvosto	**Order reference** Dnro SAFER 13/2025
Project name CFD for Reactor Safety	**Project number/Short name** 141278 / SAFER2028_CeReSa_2025
Author(s) Johanna Kapanen	**Pages** 24/
Keywords Hydrogen, Deflagration, CFD	**Report identification code** VTT-R-00113-25

Summary

Hydrogen deflagration in the THAI HD-22 and HD-23 experiments was simulated using the OpenFOAM *XiFluid* solver. The goal was to assess its accuracy in predicting flame propagation and pressure evolution in conditions relevant to hydrogen safety in nuclear reactors. The results showed good agreement with experimental data in the early combustion stages but failed to capture the later acceleration of the flame front, particularly in the downward-propagating HD-23 case. Sensitivity studies examined the effects of initial turbulence, mesh resolution, laminar flame speed correlation, internal structures, and wrinkling models. Lower turbulence levels resulted in slower combustion, and the choice of flame speed correlation influenced propagation velocity. While mesh refinement improved flame speed predictions, the wrinkling model remained mesh dependent. Modifications to the wrinkling model improved pressure agreement but did not reproduce the experimentally observed flame front shape.

Confidentiality	VTT Public

Espoo 26.3.2025

Written by

Johanna Kapanen,
Research Scientist

Reviewed by

Timo Pättikangas,
Research Team Leader

VTT's contact address
VTT Technical Research Centre of Finland Ltd, P.O. Box 1000, FI-02044 VTT, Finland

Distribution (customer and VTT)

SAFER2028 Technical Advisory Group 2.1, Johanna Kapanen (VTT), Ville Hovi (VTT), Timo Pättikangas (VTT)

Approval

VTT TECHNICAL RESEARCH CENTRE OF FINLAND LTD

Date:	31.3.2025
Signature:	
Name:	Antti Arasto
Title:	Vice President, Energy

Preface

This report describes work done in CeReSa Work Package 2 focusing on deflagration modelling with OpenFOAM *XiFluid* solver. The CeReSa project is part of the SAFER2028 programme (The Finnish Research Programme on Nuclear Power Plant Safety, 2023-2028).

This task has been funded by the National Nuclear Waste Management Fund (VYR), VTT Technical Research Centre of Finland Ltd, and Fortum Power and Heat Oy.

Espoo 26.3.2025

Johanna Kapanen

Contents

Preface 3
1. Introduction 5
2. Modelling of deflagration 5
   2.1 Progress variable approach 6
   2.2 Laminar flame speed correlations 6
   2.3 Flame wrinkling model 7
   2.4 Ignition 9
3. Case description 9
   3.1 Description of the test reactor 9
   3.2 Simulation case description 11
   3.3 Computational mesh 12
4. Results 12
   4.1 Comparison of the results to the experimental data 12
   4.2 Effect of initial turbulence 18
   4.3 Effect of laminar flame velocity 18
   4.4 Effect of internal structures 19
   4.5 Effect of wrinkling model 20
   4.6 Effect of mesh 21
5. Summary and conclusions 23
References 24

1. Introduction

Severe nuclear accidents may lead to the release of a large amount of hydrogen into containment structures. If ignited, hydrogen combustion can generate high-pressure loads and damage to the containment. Predicting the combustion behaviour of hydrogen-containing mixtures accurately is crucial for nuclear safety assessments. Hydrogen flames occurring in water-cooled containments in nuclear accident scenarios have been studied in THAI HD experiments to deal with the lack of experimental data on large test facilities and conditions typical to containments. The conditions include upward- and downward-propagating flames, elevated initial temperatures and pressures as well as relatively high steam concentrations. 29 hydrogen deflagration tests were performed in the HD programme. (Nuclear Energy Agency, 2011)

Hydrogen deflagration involves several interconnected processes, including turbulence, chemical reactions, diffusion, and thermal expansion, making its modelling complex. The flame propagates as a premixed front, where the fuel and oxidizer react, and its speed is influenced by both laminar and turbulent effects. The laminar flame speed represents the propagation rate of a smooth, undisturbed flame through a quiescent gas mixture under specific conditions (Ravi & Petersen, 2012; Gülder, 1984). In contrast, the turbulent flame speed is significantly higher due to flame wrinkling, which increases the flame surface area and enhances the overall reaction rate (Gülder 1990). As turbulence intensity grows, eddies stretch and fold the flame, leading to faster combustion.

Capturing the interaction between turbulence and flame dynamics is a major challenge in numerical simulations. Many combustion models simplify the chemical kinetics to a single-step irreversible reaction and track the flame front using a reaction progress variable. The *XiFluid* solver in OpenFOAM is designed for compressible premixed and partially premixed combustion with turbulence modeling. It employs the b-Ξ two-equation model, where Ξ represents the flame wrinkling coefficient, which can be obtained through an algebraic expression or by solving a transport equation. The flame wrinkling coefficient increases effective flame speed by incorporating turbulence-induced flame stretching and surface deformation effects. (Weller, 1993; Weller et al., 1998)

In lean hydrogen flames within low-turbulence regions instabilities such as thermal-diffusive instability and hydrodynamic instability also play a role. Thermal-diffusive instability occurs because the mass diffusivity of hydrogen is higher than its thermal diffusivity. This causes local enrichment of hydrogen in the flame front increasing reaction rates. Hydrodynamic instabilities include Darrieus-Landau instability, which results from flame wrinkling due to density changes across the flame front, and Rayleigh-Taylor instability which occurs when lighter burned gases lie below heavier unburned gases contributing to flame wrinkling. Buoyancy effects increase wrinkling in upward propagating flames while they decrease it in downward-propagating flames. (Taivassalo, 2024)

The aim of this study is to evaluate the capability of the *XiFluid* solver to predict the combustion behavior of hydrogen-containing mixtures under nuclear containment conditions. Additionally, the study will assess the sensitivity of simulation results to numerical schemes and grid resolution, ensuring reliable and accurate predictions for nuclear safety applications.

2. Modelling of deflagration

The simulations have been conducted using the *XiFluid* solver module in OpenFOAM, which employs a b-Ξ two-equation model to simulate compressible premixed and partially premixed combustion with turbulence modelling. The evolution of the flame front is described using a regress variable (b), while the turbulent flame speed is computed based on the laminar flame speed and flame wrinkling effects induced by turbulence. This approach allows the solver to account for the

interaction between turbulence and flame propagation, which is critical in hydrogen combustion scenarios.

2.1 Progress variable approach

The progress variable approach represents the flame as an infinitesimally thin interface separating burnt and unburnt gases with the transition described by a transport equation. The progress variable describes the normalized product concentration *c*. In *XiFluid*, the transport equation is solved for the regress variable *b=c-1*, the normalized fuel concentration, which takes values between 0 (fully burned) and 1 (fully unburned). The governing transport equation is given by the following equation (Weller, 1993; Weller et al., 1998):

$$\frac{\partial \bar{\rho}\tilde{b}}{\partial t} + \nabla \cdot \left(\bar{\rho}\tilde{\mathbf{U}}\tilde{b}\right) - \nabla \cdot \left(\bar{\rho}\widetilde{D_{t_b}}\nabla\tilde{b}\right) = -\overline{\rho_u}\Xi S_u\left|\nabla\tilde{b}\right| \tag{2.1}$$

where
$\bar{\rho}$ is filtered density [kg/m^3],
$\tilde{b}$ density-weighted filtered regress variable [-],
$\tilde{\mathbf{U}}$ density-weighted filtered velocity [m/s],
$\widetilde{D_{t_b}}$ density-weighted turbulent diffusivity [m^2/s],
$\overline{\rho_u}$ filtered density of the unburnt gas [-],
Ξ sub-grid flame wrinkling coefficient [-], and
S_u laminar flame speed [m/s].

2.2 Laminar flame speed correlations

The laminar flame speed is an important parameter for premixed combustion modelling, as it defines the speed at which a planar flame propagates in a quiescent mixture. It depends on the fuel-air composition, temperature, and pressure. Empirical correlations such as the power law model relate the flame speed to these thermodynamic variables (Ravi & Petersen, 2012):

$$S_u = S_{L0}\left(\frac{T_u}{T_0}\right)^{\alpha}\left(\frac{p_u}{p_0}\right)^{\beta} \tag{2.2}$$

where
S_{L0} is reference laminar flame speed at room conditions [m/s],
T_u, p_u are temperature and pressure of the unburned gas [K],
T_0, p_0 reference conditions [K], and
α, β empirical coefficients dependent on gas composition [-].

Gulder's correlation (Gülder, 1984) provides a more detailed expression for hydrogen flames:

$$S_u = W\phi^{\eta} e^{-\xi(\phi-1.075)^2} \left(\frac{T_u}{T_0}\right)^{\alpha} \left(\frac{p_u}{p_0}\right)^{\beta} \tag{2.3}$$

where ϕ is equivalence ratio [-], and
W, η, ξ are empirical coefficients dependent on gas composition [-].

The Ravi-Petersen correlation (Ravi & Petersen, 2012) uses the following polynomial fits for the parameters:

$$S_u = (a_1 + a_2\phi + a_3\phi^2 + a_4\phi^3 + a_5\phi^4)\left(\frac{T}{T_0}\right)^{b_1+b_2\phi+b_3\phi^2+b_4\phi^3} \tag{2.4}$$

where $a_1, \dots, a_4$ and $b_1 \dots, b_4$ are pressure-dependent polynomial coefficients [-].

2.3 Flame wrinkling model

In turbulent combustion, the flame front undergoes wrinkling, stretching, and folding due to turbulent eddies. These effects significantly increase the flame surface area, leading to an increase in the actual flame speed compared to laminar flame speed:

$$S_t = \Xi S_u \tag{2.5}$$

where Ξ represents the flame wrinkling coefficient. The evolution of Ξ is governed by a transport equation (Weller, 1993; Weller et al., 1998):

$$\frac{\partial \Xi}{\partial t} + \widetilde{U_s} \cdot \nabla \Xi = G\Xi - R(\Xi - 1) + (\sigma_t - \sigma_s)\Xi \tag{2.6}$$

where $\widetilde{U_s}$ is surface-filtered flame velocity [m/s],
G turbulent wrinkling generation rate [1/s],
R turbulent wrinkling removal rate [1/s],
σ_t turbulent stress term [-], and
σ_s stress due to wrinkling interaction [-].

The turbulent stress term is given by

$$\sigma_t = \nabla \cdot \left(\widetilde{\mathbf{U}} + S_u \Xi \widetilde{\mathbf{n}}\right) - \widetilde{\mathbf{n}} \cdot \left(\nabla\left(\widetilde{\mathbf{U}} + S_u \Xi \widetilde{\mathbf{n}}\right)\right) \cdot \widetilde{\mathbf{n}} \tag{2.7}$$

where $\widetilde{\mathbf{n}}$ is the direction vector of propagation.

Stress due to wrinkling interaction is given by

$$\sigma_s = \frac{\nabla \cdot \tilde{\mathbf{U}} - \tilde{\mathbf{n}} \cdot (\nabla \tilde{\mathbf{U}}) \cdot \tilde{\mathbf{n}}}{\Xi} + \left(\nabla \cdot (S_u \tilde{\mathbf{n}}) - \tilde{\mathbf{n}} \cdot (\nabla (S_u \tilde{\mathbf{n}}) \cdot \tilde{\mathbf{n}})\right) \frac{\Xi + 1}{2\Xi}. \quad (2.8)$$

The modelling of wrinkling generation and removal rate terms *G* and *R* are based on flame speed correlation by Gülder (Gülder, 1990). *G* is calculated as

$$G = R \, \frac{\Xi_{eq} - 1}{\Xi_{eq}} \quad (2.9)$$

where Ξ_{eq} is the equilibrium wrinkling coefficient [-].

Turbulent removal rate R is given by

$$R = \frac{G_\eta}{\tau_\eta} \frac{\Xi_{eq}^*}{\Xi_{eq}^* - 1} \quad (2.10)$$

where G_η is a model constant with default value 0.28 [-].

The Kolmogorov time scale τ_η is given by

$$\tau_\eta = \sqrt{\frac{\mu_u}{\rho_u \varepsilon}} \quad (2.11)$$

where μ_u is the dynamic viscosity of the unburned gas [Ns/m^2],
ρ_u the density of the unburned gas [kg/m^3], and
ε turbulence dissipation rate [m^2/s^3].

and Ξ_{eq}^* is calculated from

$$\Xi_{eq}^* = 1 + 0.62 \left(\frac{u'}{S_u}\right)^{\frac{1}{2}} R_\eta \quad (2.12)$$

where R_η is turbulent Reynolds number based on Kolmogorov length [-], and
u' turbulence intensity [m/s].

The equilibrium flame wrinkling coefficient can be calculated by a linear or a cubic profile. Equilibrium coefficient calculated by a linear profile is given by

$$\Xi_{eq} = 1 + (1 + \Xi_{\text{coeff}} * 2(0.5 - b))(\Xi_{eq}^* - 1) \quad (2.13)$$

where Ξ_{coeff} is a model coefficient with a default value 1.

Equilibrium coefficient calculated by a cubic profile is given by

$$\Xi_{eq} = 1 + \left(1 + \Xi_{\text{coeff}} * \left(2(0.5 - b)\right)^3\right)(\Xi_{eq}^* - 1) \quad (2.14)$$

The wrinkling can be modelled also with an equilibrium model which uses an algebraic expression from equations 2.12-2.14 without a transport equation.

2.4 Ignition

Combustion is initiated by an ignition process, which introduces a localized energy source to trigger the flame kernel formation. In the numerical model, this is achieved by adding a source term to the transport equation of the regress variable b within a predefined ignition region. This source term modifies the unburned gas fraction over the ignition period, simulating the development of a flame kernel.

The ignition source term is defined as:

$$S_p = -\frac{V_c \rho_u strength}{\Delta t * b} \quad (2.15)$$

where V_c is volume of the ignition region [m^3],
ρ_u convective mixture molar flux [m^3/s],
$strength$ a model parameter that controls the ignition intensity [1/s] and
Δt duration of the ignition phase [s].

A correction term for Ξ is also included in the ignition model to ensure that the turbulent flame speed enhancement reflects the actual flame kernel geometry during ignition, especially in the early stages when the kernel is not fully developed (does not have a completely burnt side). During ignition, the flame kernel's surface area can be underestimated due to coarse resolution or non-uniform flame propagation.

3. Case description

3.1 Description of the test reactor

The simulated cases, THAI HD-22 and HD-23 are a part of a series of hydrogen deflagration tests performed in the Thermal-Hydraulics Hydrogen Aerosols (THAI) test facility, operated by Becker Technologies GmbH at Eschborn, Germany. These experiments aim to improve the understanding of hydrogen combustion dynamics under conditions relevant to severe nuclear accidents.

The test vessel, illustrated in Figure 1, is a vertically oriented, insulated cylinder chamber with an internal height of 9.2 m and an internal diameter of 3.2 m, resulting in a total volume of 60 m^3. The vessel is initially filled with a homogeneous gas mixture of hydrogen (H_2), steam (H_2O) and air. In THAI HD-22 test the gas is ignited from the bottom and flame propagates upwards after ignition while in THAI HD-23 test the ignition is at the top. (Nuclear Energy Agency, 2011)

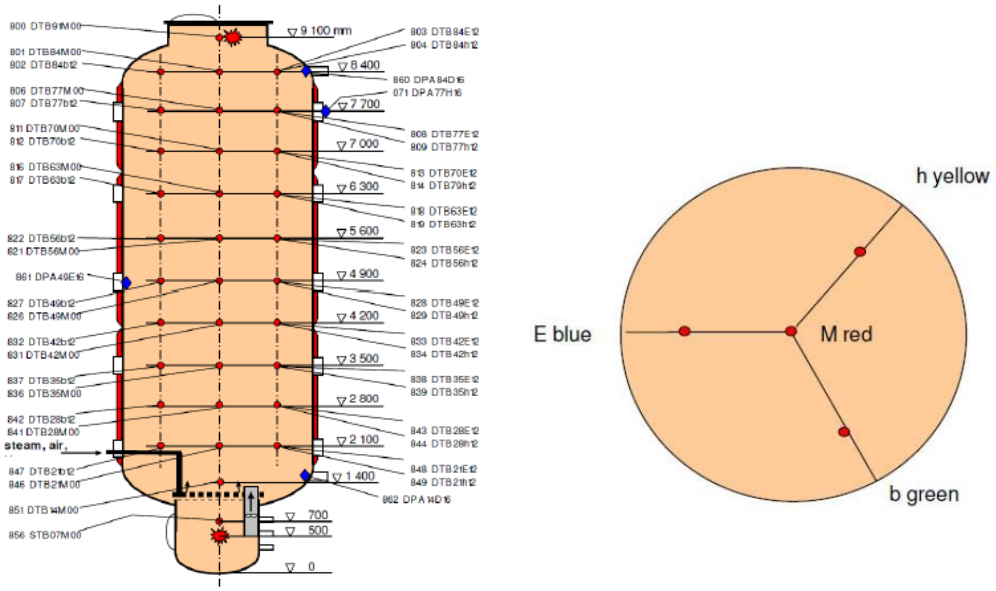

Figure 1. The geometry of the THAI vessel with locations for top and bottom ignition and measurement instrumentation. Measurement points are placed at 120° intervals at 1.2 m radius on each measurement height. (Nuclear Energy Agency, 2011)

Before the combustion experiment, the reactor is preheated to 90 °C. Steam and hydrogen are injected into the vessel and mixed with the air in the reactor with a fan blower to ensure homogeneity. The initial mixture composition, pressure and temperature are summarized in Table 1. The mixture is ignited by an igniter positioned in the THAI-HD 23 test case at the top of the vessel at 9.1 m height, 15 cm off the centre axis. In the THAI HD-22 test case the igniter is at 0.5 m height at the vessel centreline.

Table 1. Initial conditions of the THAI HD-22 and HD-23 cases.

	THAI HD-22	THAI HD-23
Initial temperature (°C)	90	91
Initial pressure (bar)	1.49	1.47
Equivalence ratio	0.36	0.45
H_2 volume fraction (%)	9.9	12
H_2O volume fraction (%)	25	25
Air volume fraction (%)	65	63

Initial turbulence parameters were not directly measured in the THAI-HD tests. However, since ignition occurs 10-15 minutes after the end of the fan operation, the initial turbulence level can be assumed to be low.

The thermal boundary conditions of the vessel are controlled using a thermal oil system that cools and heats the cylindrical walls, while the top and bottom sections are insulated with a 120 mm thick rock wool layer. These thermal conditions influence the heat transfer between the flame and the vessel walls, affecting the combustion process.

3.2 Simulation case description

The gas mixture is modeled as a homogeneous mixture of fuel, oxidizer, and combustion products where the regress variable depicts the fraction of the unburned fuel and oxidizer and burned products. In the case of the THAI HD-23 case, the fuel consists of 100% hydrogen (H_2), while the oxidizer is composed of 28.7% steam (H_2O), 15.0% oxygen (O_2), and 56.3% nitrogen (N_2). The products consist of 39.6% steam, 7.7% oxygen and 52.7% nitrogen. The thermodynamic and transport properties of the fuel, oxidizer and products are determined using JANAF polynomials.

Ignition is initiated in both cases at 0.05 s using a constant ignition model with an ignition strength of 2 and a duration of 0.0005 s. To assess the impact of ignition parameters on combustion dynamics, an additional sensitivity study is conducted with varying ignition strengths. The laminar flame speed is computed using the Ravi-Petersen correlation. Gülder correlation is also used in the sensitivity study to examine the effect of laminar flame speed correlation on flame propagation. The flame wrinkling coefficient (Ξ) is calculated using a transport model based on Gülder's approach. To further investigate the influence of turbulence-chemistry interaction, different models for Ξ have been tested.

Turbulence is modeled using the k-ω-SST model, with an initial turbulent kinetic energy (k) of 0.005 m^2/s^2 and an initial specific dissipation rate (ω) of 1 s^{-1}. Since the initial turbulence level in the THAI HD tests was not measured, these values are chosen to represent low initial turbulence. A sensitivity study has been performed by modifying the initial k value to evaluate its effect on flame propagation. The impact of computational grid resolution on the results has also been assessed by performing simulations with both a coarser and a finer mesh.

The vessel is assumed to be empty in the reference case, with no internal structures included in the mesh. However, as seen in Figure 2, the actual test vessel contains several instrumentation-related structures that may generate turbulence during combustion. To examine their potential effect on flame wrinkling and propagation speed, an additional case has been simulated with these internal structures included.

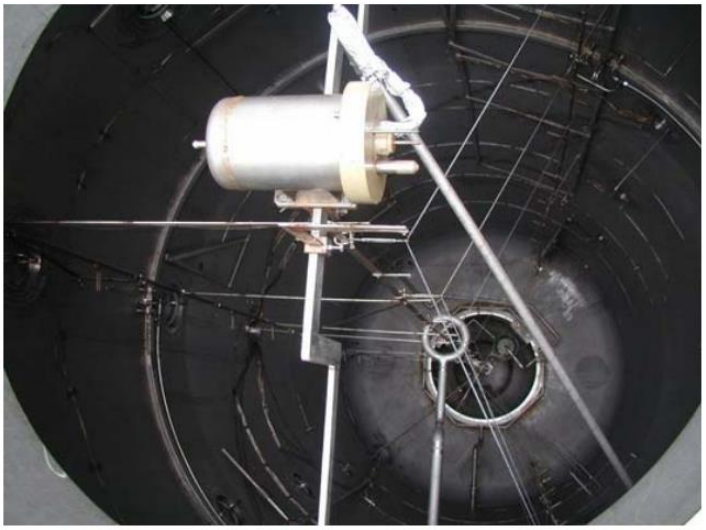

Figure 2. Internal structures of the THAI test vessel. (Nuclear Energy Agency, 2011)

Radiation heat transfer is modeled using the discrete ordinates (DO) method, with wall emissivity set to 1. The cylindrical vessel walls are thermally controlled and assumed to remain at the initial temperature of 90°C, while the top and bottom sections are considered adiabatic.

These modelling assumptions and sensitivity studies provide a comprehensive evaluation of the key parameters affecting the hydrogen deflagration process in the test reactor.

3.3 Computational mesh

The computational mesh for THAI HD-23 case is a polyhedral mesh with an extruded cylindrical section with 1.84 million cells and a mean cell size of 4 cm. The area near the ignition point is refined with a 2 cm cell size. The mesh for the THAI HD-22 case is similar but the refined ignition area is at the bottom of the vessel. The meshes are shown in Figure 3.

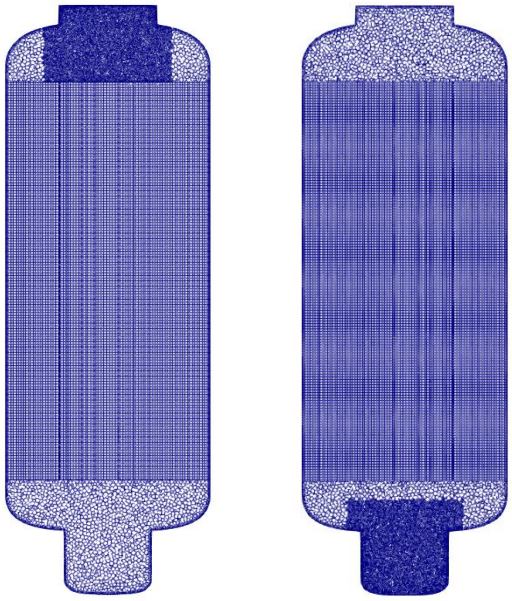

Figure 3. The computational meshes for THAI HD-23 (left) and THAI HD-22 (right) simulations.

The HD-23 case is also simulated with two additional meshes to assess the mesh-dependency of the results. A coarser mesh with 295,000 cells and a mean cell size of 6 cm with no cell refinement in the ignition region. Additionally, a finer mesh with 3.6 million cells is employed with increased refinement near the ignition region and along the vessel walls.

4. Results

The THAI HD-22 and HD-23 test cases were simulated and the results compared to measurements. The sensitivity of the model to different parameters was studied for the THAI HD-23 test case. The parameters varied in the sensitivity study included the initial turbulence kinetic energy, ignition strength, mesh resolution with coarser and finer grids, laminar flame speed using both Ravi and Gulder correlations, inclusion of internal structures, and testing of several models for the wrinkling factor Ξ.

4.1 Comparison of the results to the experimental data

Figure 4 shows isochrones describing the flame propagation through the test vessel in the two experimental cases. The figure shows that in the downward propagating flame, at the initial stages, the flame front is convex and symmetrical evolving to an unsymmetrical concave shape closer to the vessel bottom. The upward propagating flame is more concave and stays quite symmetrical throughout the propagation.

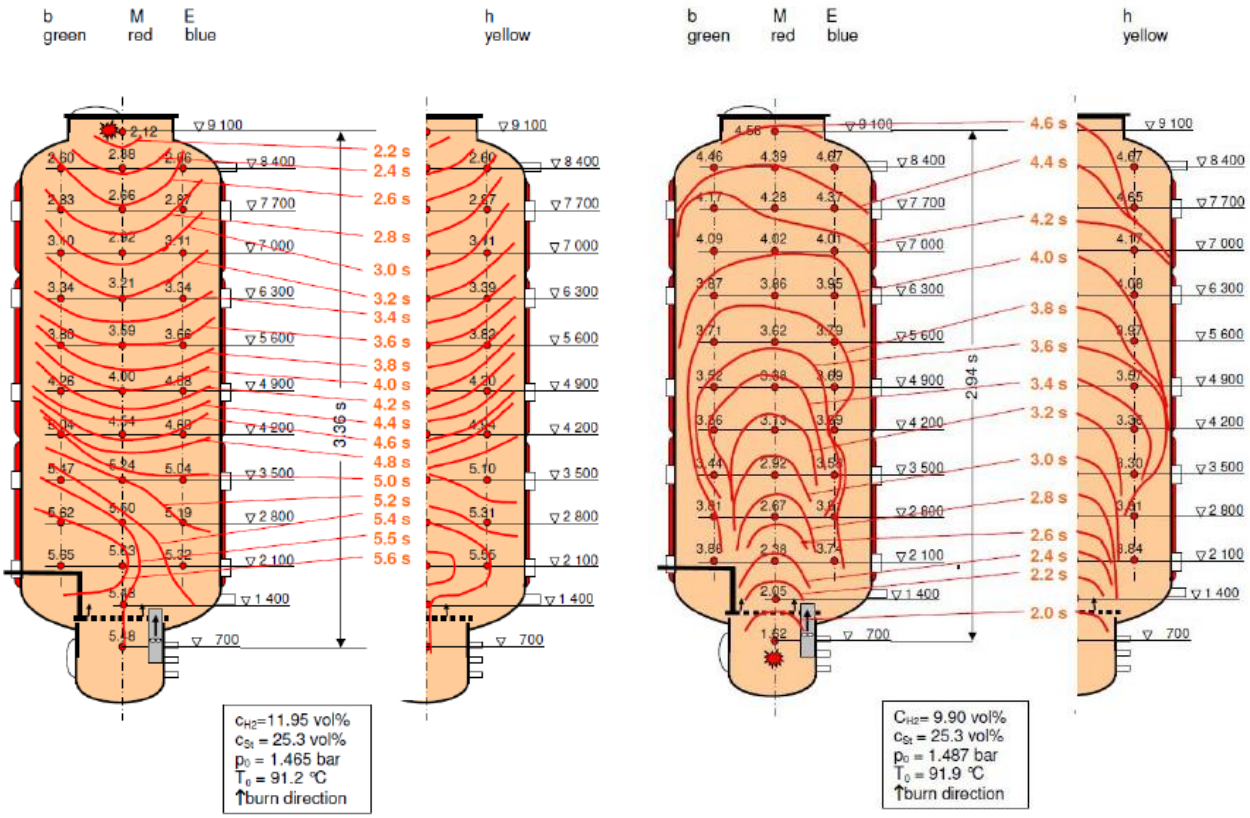

Figure 4. THAI HD-23 (left) and HD-22 (right) flame front propagation as isochrones. The location of measurement point sets green, red, blue and yellow correspond to the ones in Figure 1. (Nuclear Energy Agency, 2011)

The pressure evolution in the two experimental cases and the simulations are shown in Figure 5. The upward propagating flame has a slow starting period after which the flame front accelerates. The downward propagating flame front has a higher velocity at the first stage, but the flame front accelerates later during the combustion process and the total combustion time is higher compared to the upward propagating flame. After combustion, the pressure decreases due to cooling of the vessel walls.

The simulations agree quite well with the measurements in the beginning of the combustion while the flame speed in the latter part of the combustion is underestimated in both cases. While the model fails to capture the acceleration of the flame front at the mid stage of the combustion in both cases, the error is more pronounced in the downward-propagating flame. Also, the pressure peak at the end or the combustion is wider in the simulations compared to the experiments where the pressures decrease rapidly after the peak pressure is reached.

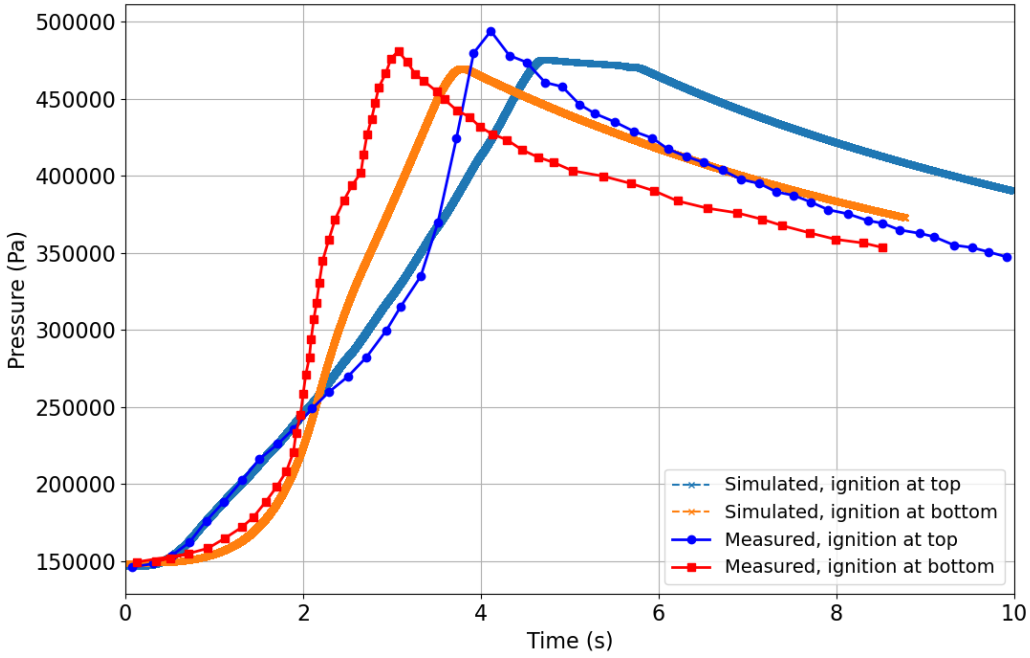

Figure 5. The pressure transient in experimental flames and simulated cases.

Figure 6 shows the flame arrival times on four different lines along the vessel length in THAI HD-23 test case. The location of these lines can be seen in Figure 1. The figure shows that the simulation agrees well with the measurement in the beginning at the centreline but the discrepancy between the two increases with increasing time especially in lines 2-4. The different measured flame arrival times at the centreline and lines 2-4 show that the flame shape is convex while the simulation results indicate a planar flame shape which can also be seen in Figures 7-10.

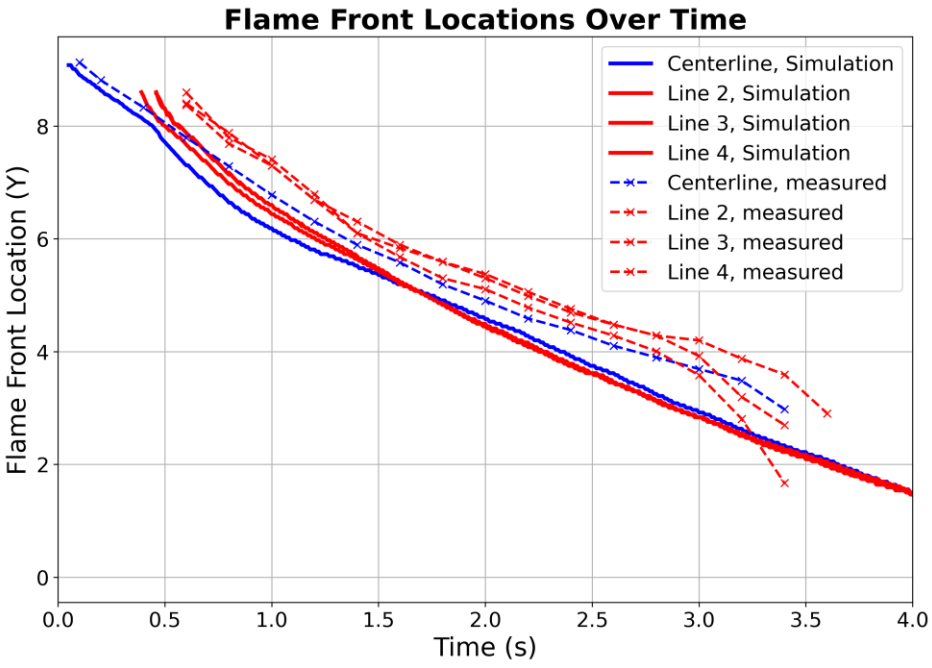

Figure 6. Computational and experimental flame arrival times in THAI HD-23 case on four different lines along the vessel length. (Xiao & Jordan, 2018)

The propagation of the flame in THAI HD-23 case is shown in Figures 7-10. The figures show the evolution of regress variable, flame wrinkling coefficient, temperature and vertical gas velocity in the test vessel. The figures show that after ignition, the flame front shape is concave like in the experiments. However, the simulated flame front takes a planar shape earlier than the experimental flame. This means that the velocity of the flame front is too slow at the centreline of the vessel. Furthermore, the unsymmetrical shape of the flame front at the latter part of the combustion is not captured by the model. The flame front values of the wrinkling coefficient, shown in Figure 8, increase throughout the combustion process ranging from 1 to 2.

The gas temperature, shown in Figure 9, is quite constant, around 1000 °C in the burned region with near-wall regions cooling down. The vertical velocity in Figure 10, shows upward velocity of the expanding lighter burned gas in the vessel centre and downward velocity for the cooler gas in the near-wall region. At the latter part of the combustion, an area develops near the centreline where velocities are close to zero.

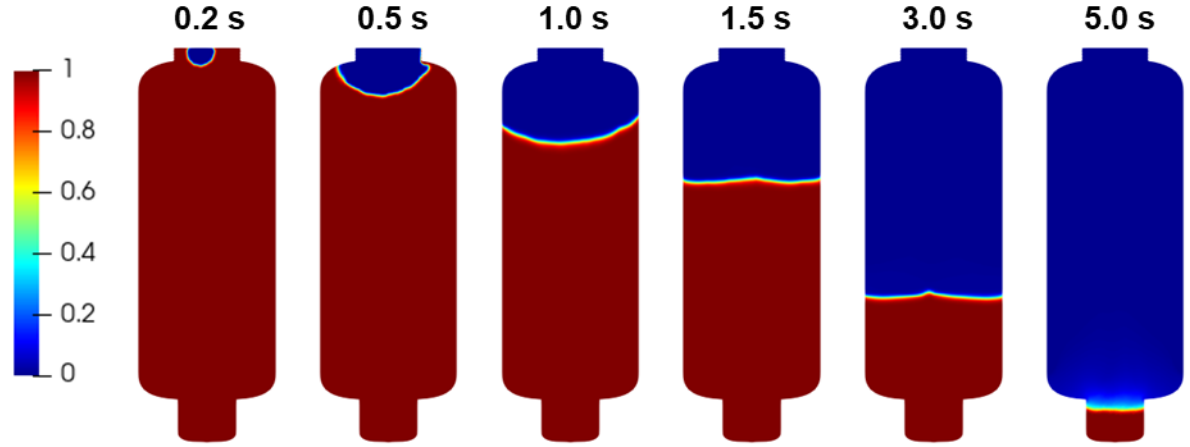

Figure 7. Simulated reaction regress variable b at different times in THAI HD-23 test.

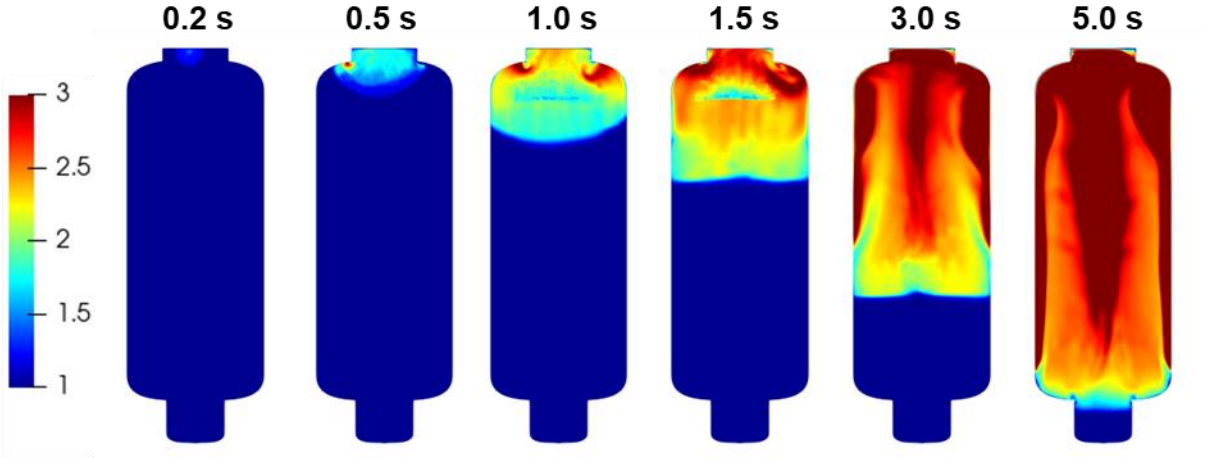

Figure 8. Simulated wrinkling coefficient Ξ at different times in THAI HD-23 test.

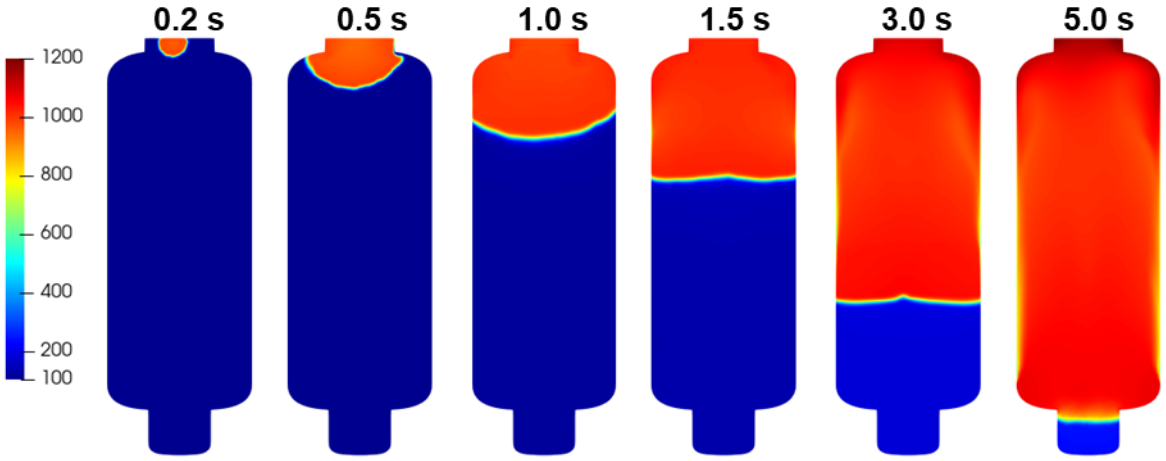

Figure 9. Simulated temperature [°C] at different times in THAI HD-23 test.

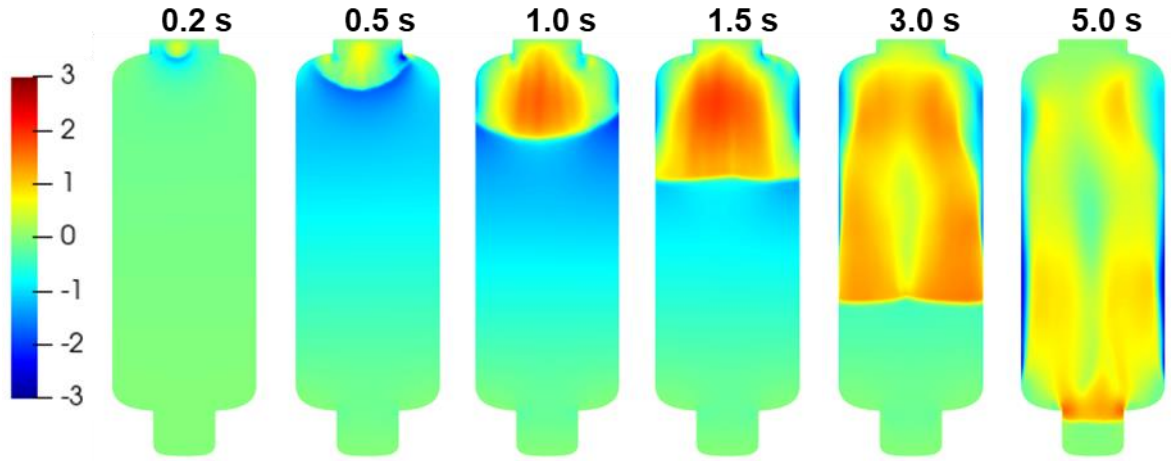

Figure 10. Simulated vertical velocity [m/s] at different times in THAI HD-23 test.

The evolution of the simulated flame front in THAI HD-22 case is shown in Figures 11-14. The flame front (Figure 11) takes a more convex shape which is kept throughout the combustion process.

The temperature (Figure 13) of the burned mixture in the HD-22 case is 800-900 °C which is lower than in the HD-23 case. The upward gas velocity, shown in Figure 14, is around 6 m/s at the vessel centreline with the cooler gas flowing downwards near the walls. The velocity levels are much higher compared to the downward-propagating flame which increases turbulence and the wrinkling of the flame (Figure 12).

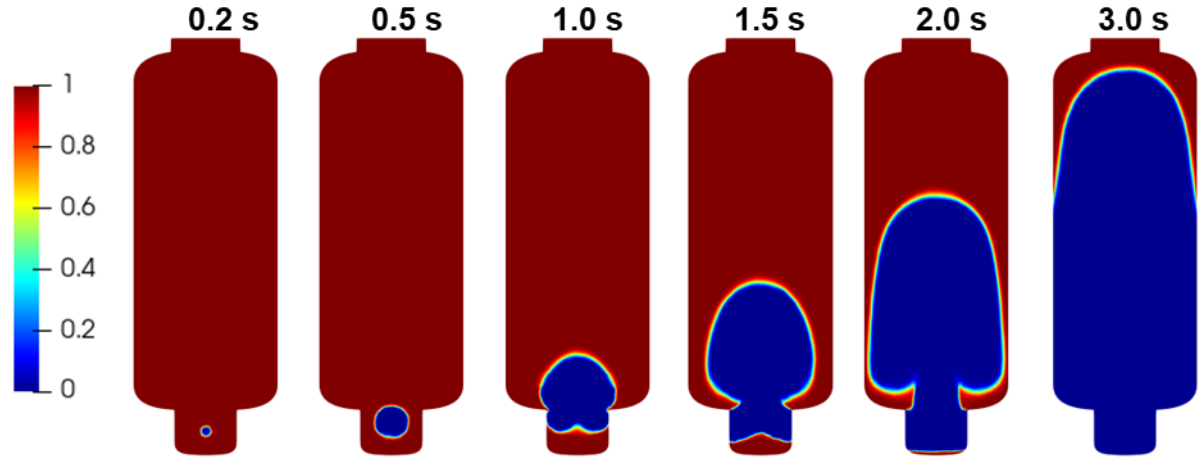

Figure 11. Simulated reaction regress variable b at different times in THAI HD-22 test.

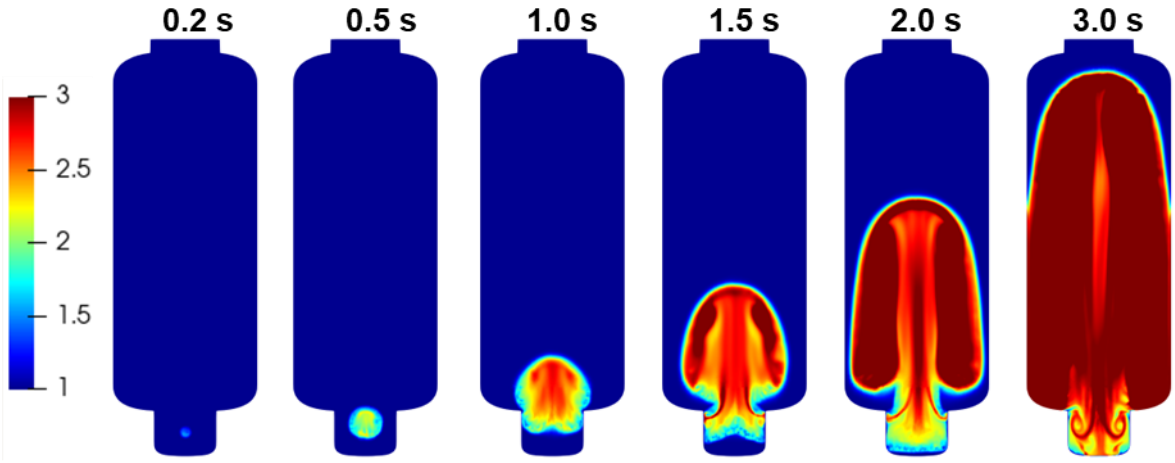

Figure 12. Simulated wrinkling coefficient Ξ at different times in THAI HD-22 test.

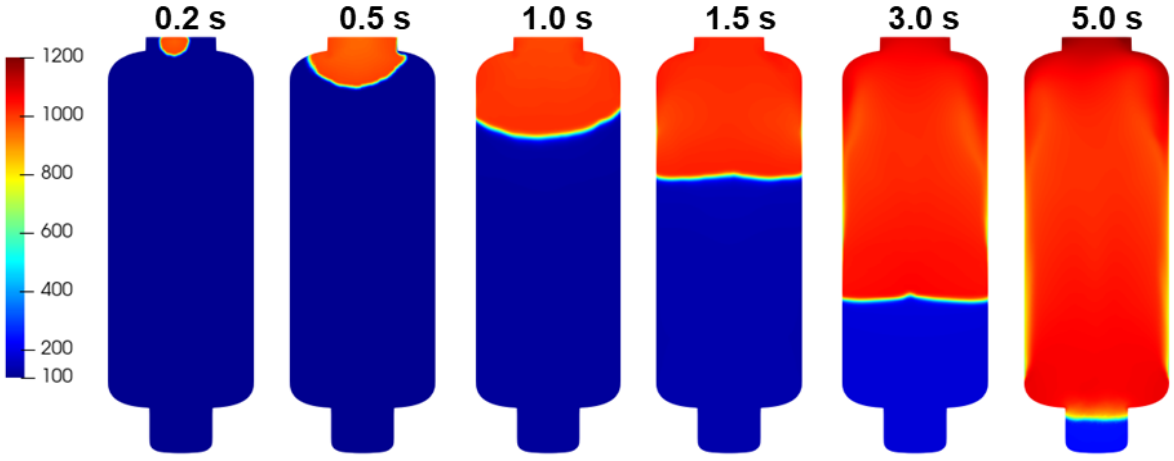

Figure 13. Simulated temperature [°C] at different times in THAI HD-22 test.

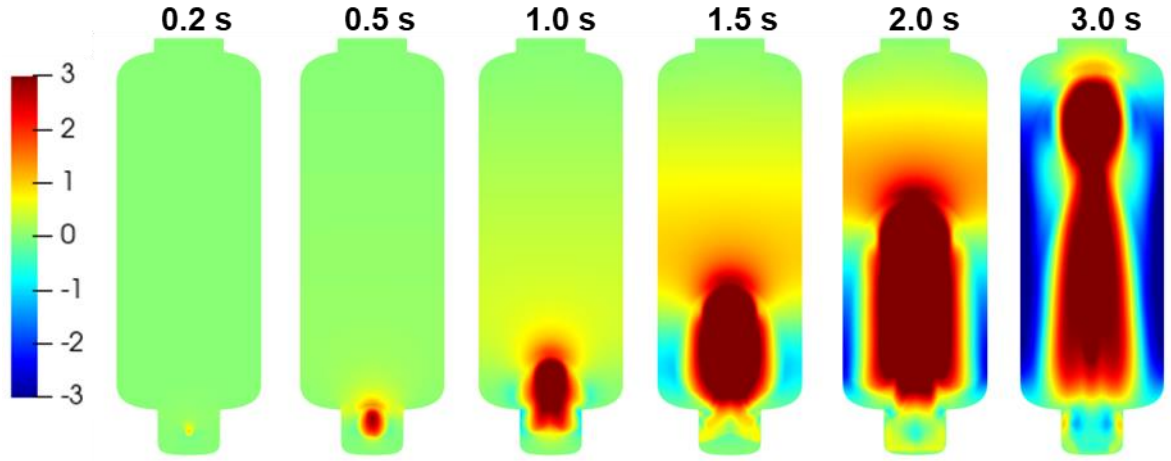

Figure 14. Simulated vertical velocity [m/s] at different times in THAI HD-22 test.

4.2 Effect of initial turbulence

In the THAI HD-23 test case, the effect of initial turbulence level on hydrogen deflagration was analysed by changing the initial turbulence kinetic energy from 0.005 to 0.001. A lower initial turbulence level resulted in a slower combustion process because the reduced turbulence intensity limits the increase of the flame surface area and mixing. This effect was noticeable in the later stage of combustion, where the flame speed was slower compared to the higher turbulence case.

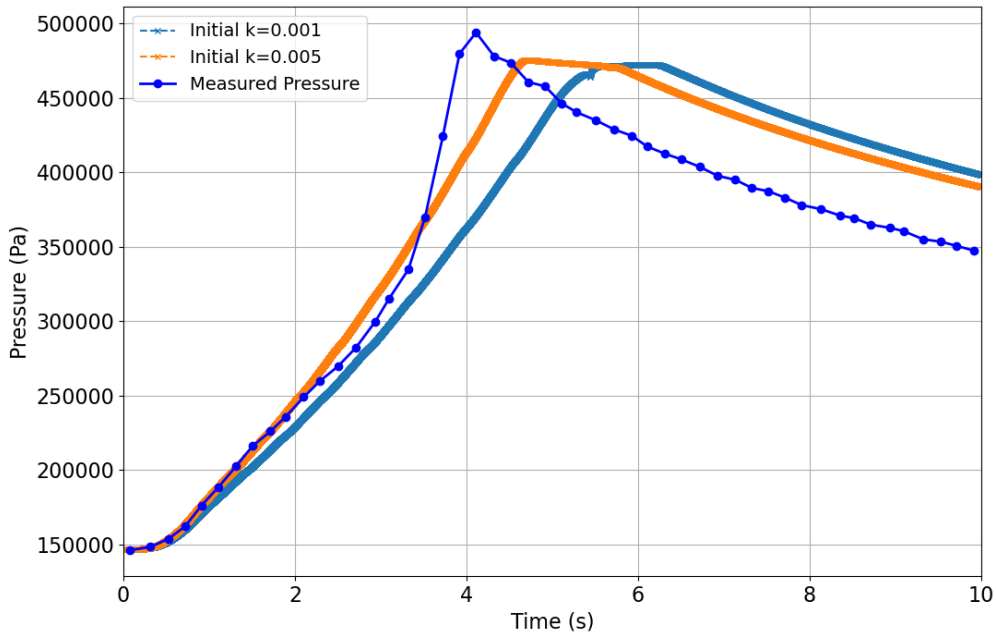

Figure 15. The effect of initial turbulence intensity on pressure transient.

4.3 Effect of laminar flame velocity

The effect of laminar flame speed model was studied by simulating the THAI HD-23 case with Gulder model. The choice of flame speed model has an impact on the simulation results. The Ravi-Petersen

model, used as the reference case, produces higher flame propagation velocity, while the Gulder correlation gives slower flame propagation, particularly in the later stages of combustion.

Both models are designed for pure H_2-air mixtures, while in the THAI HD cases there is initial H_2O in the gas mixture, which may affect the reactivity of the gas. This omission may cause an error in the flame speed, particularly in the early stages of combustion. However, both flame speed correlations consider the equivalence ratio, thus accounting for the diluting effect of the H_2O.

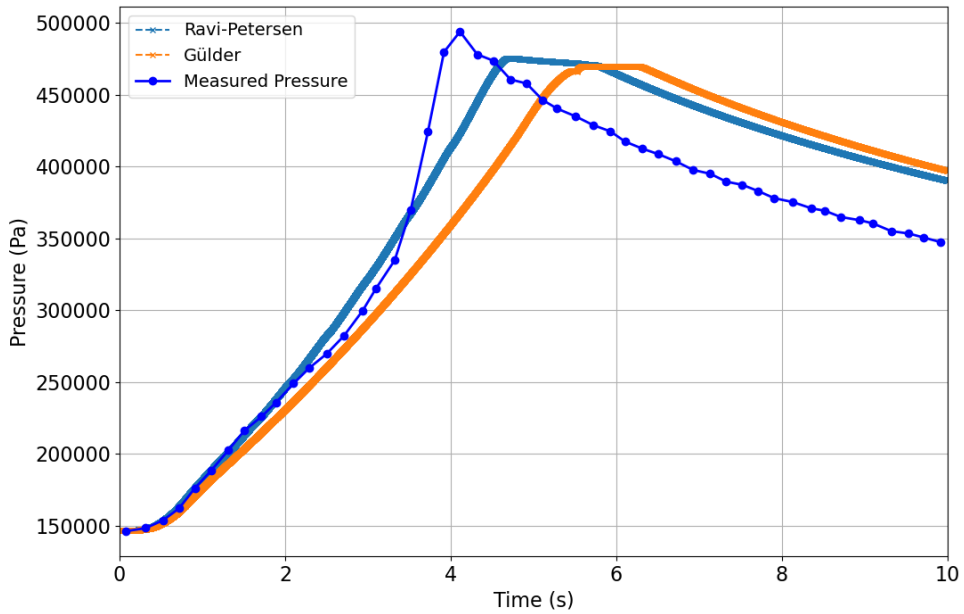

Figure 16. The effect of changing the laminar flame speed correlation from Ravi-Petersen to Gülder on the pressure transient.

4.4 Effect of internal structures

The presence of measurement instrumentation means that the vessel is not completely empty as is initially assumed in the simulations. Internal structures were added to the computational mesh to account for their potential effect on turbulence. The effect of the structures can be seen in Figure 17 which shows minimal impact on the flame speed.

The structures were introduced to the mesh with no refinement or boundary layers around them which may result in an underestimation of the turbulence they generate. A finer mesh could potentially capture turbulence effects better. However, the negligible impact on flame speed suggests that the presence of measurement instrumentation may not significantly influence flame propagation in the vessel.

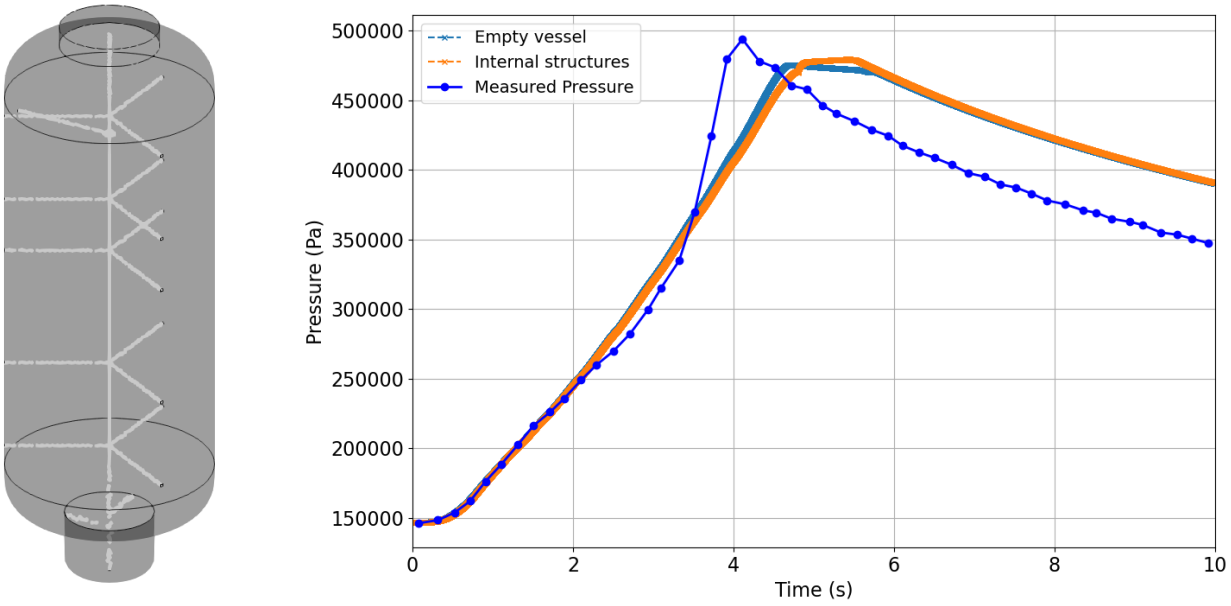

Figure 17. The internal structures added to the computational geometry and the effect of the structures on the pressure transient.

4.5 Effect of wrinkling model

Since the wrinkling model used in the simulations fails to capture the acceleration of the flame front in the later stages of combustion, modifications to the model coefficients were tested to improve accuracy.

The first modification involved increasing the G_η coefficient from 0.28 to 1.5 in Equation 2.10 to increase the wrinkling generated by turbulence. The second adjustment increased the Ξ_{coeff} in Equations 2.13 and 2.14 from 1 to 2.5. The third change involved altering the Ξ_{eq} profile from a linear formulation (Equation 2.13) to a cubic one (Equation 2.14). Additionally, a case with a constant wrinkling coefficient of 1.5 was simulated. The different wrinkling models and their coefficients used in the simulated cases are listed in Table 2.

Table 2. Different wrinkling models and their coefficients simulated in the sensitivity study.

	Ξ model	**Ξ Profile**	**Ξ_{coeff}**	**G_η**
Default model	Transport	Linear	1	0.28
Modified Ξ v1	Transport	Linear	2.5	1.5
Modified Ξ v2	Transport	Cubic	2.5	1.5
Constant Ξ = 1.5	Constant	-	-	-

The pressure profiles in the calculated cases are shown in Figure 18. Using a constant wrinkling coefficient Ξ=1.5 gives an increased constant flame front velocity throughout the combustion process that is overestimated compared to the experimental measurements.

The simulations with modified wrinkling model coefficients show improved agreement with the experiments with a slower initial propagation phase followed by and accelerated end. However, the cooling down period remains delayed compared to the measurements in all the simulated cases. The cubic model leads to an overestimation of peak pressure by 0.5 bar. Additionally, the cubic formulation is very sensitive to the chosen model constants which may lead to unpredictable results under different conditions. Despite the adjustments made, none of the models reproduce the concave flame front shape observed in experiments and shown in Figure 4.

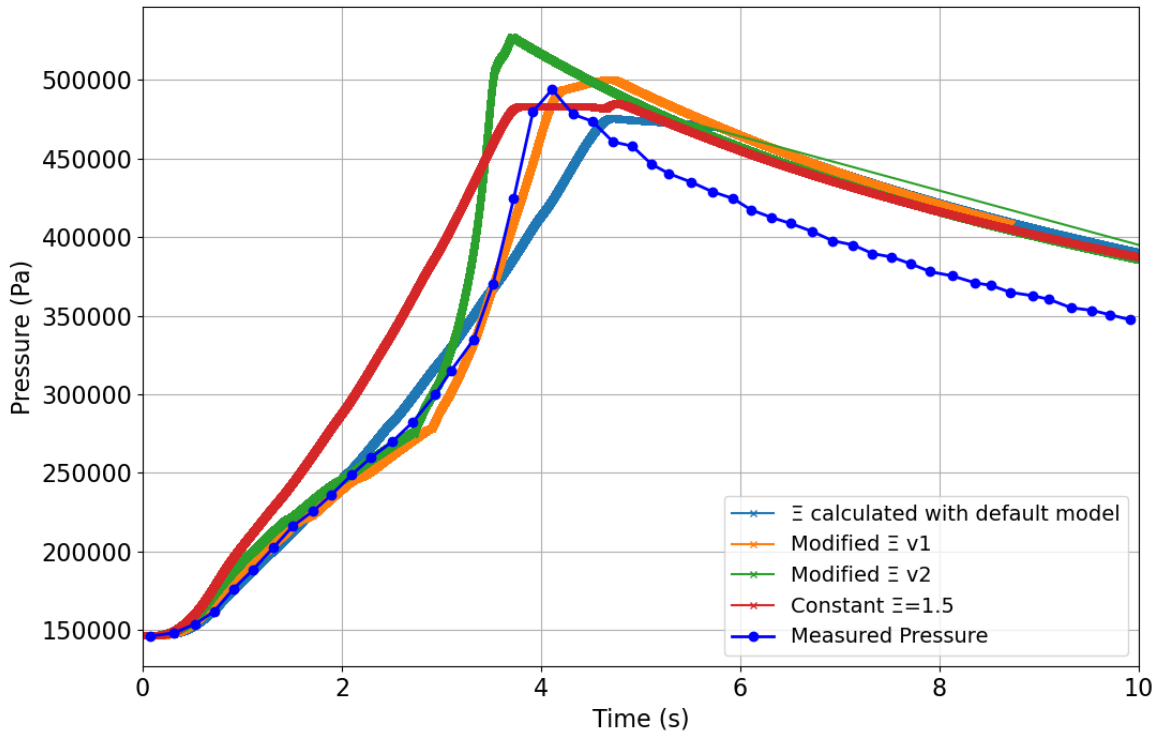

Figure 18. The effect of modified wrinkling model to the pressure transient.

4.6 Effect of mesh

Three different mesh resolutions were used in the simulations. The coarse mesh consisted of 290,000 cells, while the reference case contained 1.84 million cells. The finest mesh had a total of 3.6 million cells.

The pressure curves, shown in Figure 19, indicate that the results remain mesh-dependent even after refining the mesh from 1.84 to 3.6 million cells. The flame propagation speed increases with higher mesh resolution, suggesting that finer meshes better capture the small-scale turbulence and flame wrinkling effects. Additionally, it was observed that a coarse mesh in the ignition region can lead to incomplete ignition, causing the regress variable *b* to remain at values above 0. This results in lower simulated pressures compared to experiment that than be seen in the pressure evolution for the coarse mesh.

To further investigate the effect of the mesh, simulations were also performed using a constant wrinkling coefficient of Ξ = 1.5 resulting in simulation results independent of mesh resolution. This

indicates that only the modelling of wrinkling and its transport is mesh-dependent while the rest of the solution is not.

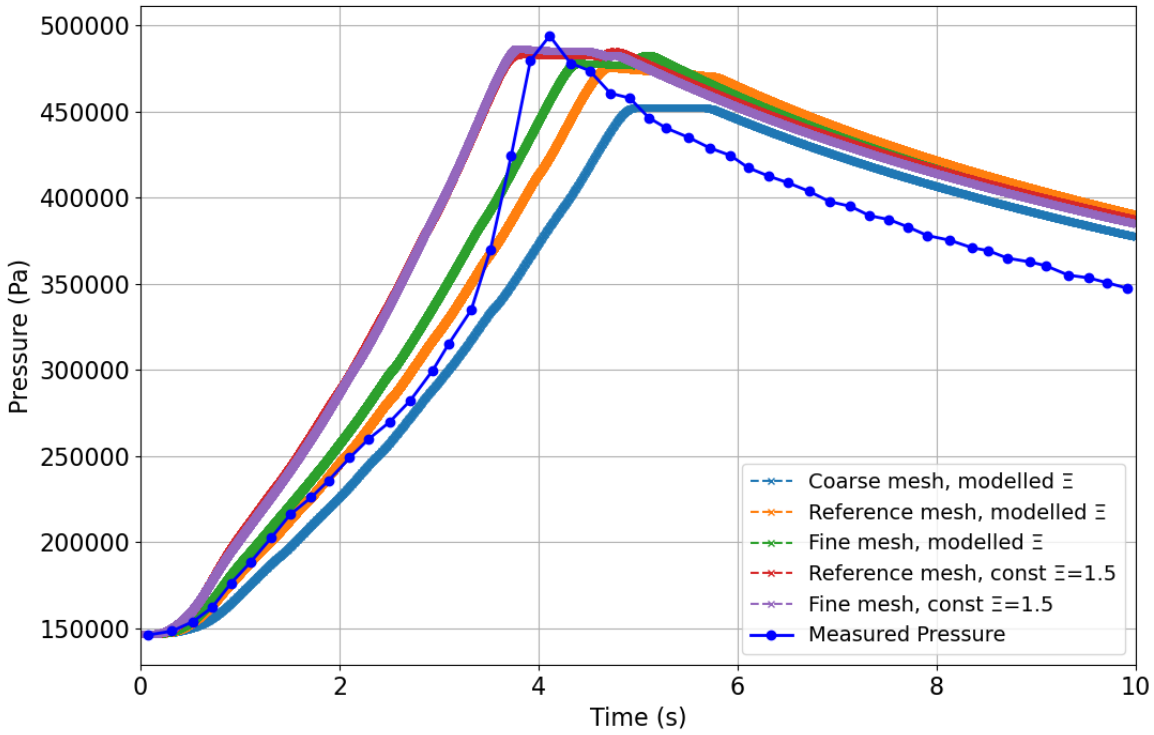

Figure 19. The effect of mesh resolution to the pressure transient with modelled and constant wrinkling coefficients.

5. Summary and conclusions

The simulation of hydrogen deflagration experiments in the THAI HD-22 and HD-23 cases using the OpenFOAM *XiFluid* solver showed reasonably good agreement with experimental data in the early stages of combustion. However, the model failed to fully capture the acceleration of the flame front in the later phases, particularly in the downward-propagating flame in HD-23. This suggest that the wrinkling model underestimates the generation of wrinkling during the progression of the flame front. The predicted pressure peak was also not entirely accurate, with the simulations showing a broader pressure peak compared to the rapid pressure drop observed in the experiments after the peak pressure.

The sensitivity study showed the impact of several relevant factors. Lower initial turbulence levels resulted in slower combustion due to reduced flame wrinkling and mixing, showing that the initial conditions strongly influence the results. However, switching from k-ω SST turbulence model to k-ω SST-SAS did not affect the results. The choice of laminar flame speed correlation also affected the predictions, with the Ravi-Petersen model producing faster flame propagation than the Gulder correlation. The inclusion of internal structures to the computational domain had minimal influence on overall flame propagation, although the turbulence generated by these structures may have been underestimated due to the lack of mesh refinement around them. The effect of ignition strength was also tested but did not seem to have a significant effect on the results.

The modifications to the wrinkling model improved the agreement with pressure measurements but did not reproduce the concave flame front shape observed in experiments. The cubic formulation of the wrinkling factor led to an overestimation of the peak pressure and was highly sensitive to the chosen model constants, making it less reliable for predictive simulations.

Mesh resolution also had a noticeable effect on the results, with finer grids leading to higher flame speeds probably due to improved resolution of small-scale turbulence and flame wrinkling. The results indicate that the modelling and transport of the wrinkling coefficient Ξ is the mesh dependent part of the model. The results remained mesh-dependent even at the highest resolution of 3.6 million cells, indicating that further mesh refinement or model improvements may be necessary for full numerical convergence of the wrinkling model. A simulation with a coarse mesh may underestimate the flame surface area, leading to slower flame propagation, while numerical dissipation can reduce wrinkling and the turbulent flame speed.

A key limitation of the current model is that it does not account for instabilities that may play an important role in low-turbulence cases such as the THAI HD-22 and 23 tests. These instabilities could contribute to the acceleration of the flame front, which was underestimated in the simulations. Future work should focus on improving the wrinkling model. Further refinement of the mesh could help reduce numerical dissipation and better resolve flame structures. Addressing these issues would improve the capabilities of the model for simulating hydrogen deflagration in conditions relevant to nuclear safety.

References

Gülder, Ö. 1984. Correlations of laminar combustion data for alternative SI engine fuels. SAE technical paper No. 841000.

Gülder, Ö. 1990. Turbulent Premixed Flame Propagation Models for Different Combustion Regimes. Twenty-Third Symposium (International) on Combustion/The Combustion Institute. pp. 743-750.

Nuclear Energy Agency. 2011. *International Standard Problem ISP-49 on Hydrogen Combustion*. NEA/CSNI/R(2011)9. OECD Nuclear Energy Agency.

Ravi, S. and Petersen, E. 2012. Laminar flame speed correlations for pure-hydrogen and high-hydrogen content syngas blends with various diluents. International Journal of Hydrogen Energy. Volume 37, Issue 24, pp. 19177-19189.

Taivassalo, V. 2024. Flame wrinkling factor in quiescent hydrogen-air mixtures. Nuclear Engineering and Design, Volume 421, pp. 113031.

Weller, H. 1993. The Development of a New Flame Area Combustion Model Using Conditional Averaging. Thermo-Fluids Section Report TF/9307. Department of Mechanical Engineering. Imperial College London.

Weller, H., Tabor, G., Gosman, A., and Fureby, C. 1998. Application of a Flame-Wrinkling LES Combustion Model to a Turbulent Mixing Layer. Twenty-Seventh Symposium (International) on Combustion, 899-907. The Combustion Institute.

Xiao, J. and Jordan, T. 2018. Numerical Investigation of Downward-propagating Hydrogen Flame in THAI HD-23 Test Using CFD Code GASFLOW-MPI. CFD4NRS-7: OECD/NEA & IAEA Workshop Application of CFD/CMFD Codes to Nuclear Reactor Safety and Design and their Experimental Validation. Shanghai, China.